Journal of Turbulence
Vol. 00, No. 00, 2011, 1–16

Two-dimensional numerical simulations of particle bed scour by repeated impacts of a vortex pair

Dan Hagan[a],Yves Dubief[a*],Mandar Dewoolkar[b],Olivier Desjardins[c]

[a]*School of Engineering, Mechanical Engineering Program, University of Vermont, Burlington, VT 05405, USA*, [b]*School of Engineering, Civil and Environmental Engineering Program, University of Vermont, Burlington, VT 05405, USA*, [c]*Sibley School of Mechanical and Aerospace Engineering, Cornell University, Ithaca, NY 14853, USA*,
(*Received December 2014*)

The repeated impacts of a vortex dipole on a particle bed are modeled using a highly resolved Euler-Lagrange simulation code. The scour characteristics and flow dynamics are investigated for a range of Shields parameters. The vortex dipole propagates perpendicularly to the particle bed, and, for all Shields parameters above the critical value, results in the scouring of the bed and eventual dissipation of the dipole. After completion of the scour event, the simulation is repeated, where subsequent simulations use the scoured bed from the previous simulation as the new initial bedform. The evolution of the scoured beds reveal that, although the scour hole shape continues to evolve with repeated impacts of the dipole, the scour hole depth asymptotically reaches a maximum. Additionally, once the scour hole reaches a critical depth, it can act to restrict the motion of the vortices after their initial interaction with the bed.

Keywords: Erosion, vortex pair, sediment bed, direct numerical simulation.

1. Introduction

The erosion of a sediment bed by flowing water, also known as the scour process, is the fundamental process behind losses of bridges, roads and shorelines particularly during dramatic weather patterns (floods, hurricanes, etc). The fluid mechanics research community has a long standing interest in the process, ranging from the formation of topographical scour patterns [1–4] to mathematical scour models [5]. The bulk of the research has mostly been focused on erosion processes over long time-scale, where the flow is at or near equilibrium. Slow scour processes can adequately be investigated with Reynolds Averaged Navier-Stokes (RANS) simulation thanks to the equilibrium nature of the turbulence in the flow. Yet in the aforementioned natural catastrophes, one should expect strong non-equilibrium effects arising from the dynamic interactions between the eroding flow and the erodible surface. In such events, characterized with large flow rates, it is fair to assume that the flow is turbulent or at least transitional. Turbulence consists of coherent structures whose topologies, scales and intensities are driven by boundary conditions. In the case of wall flows, the two basic coherent structures found near the wall are quasi-streamwise vortices and streaks (regions of locally high or low speed flows elongated in the streamwise direction). These structures combined with the wall shear stress form an autonomous cycle that sustain turbulence [6]. Since scour is the result of a mechanical erosion exerted by the flow on the sediment bed, it is safe

*Corresponding author. Email: ydubief@uvm.edu

ISSN: 1468-5248 (online only)
© 2011 Taylor & Francis
DOI: 10.1080/14685248.YYYYxxxxxx
http://www.tandfonline.com

to assume that coherent structures must be a critical component of the erosion of a sediment bed by a turbulent flow. Coherent structures over an erodible wall induce a modification of the wall boundary conditions through topographic changes. If the surface develops significant roughness and/or recedes fast, the coherent structures are expected to respond to the new boundary conditions, which in turns may locally modify the flow and therefore the erosion rate.

We speculate that the dynamic interplay between coherent structures and erodible walls is the cornerstone of the non-equilibrium effects in fast erosion rate events. This interplay has received some attention in the literature, with models for the erodible wall ranging from Eulerian scalar concentrations to immersed boundaries (IB) and Lagrangian particle tracking (LPT), which is used in this work. As IB and LPT methods have become more mature, they have been used to simulate many canonical particle-flow configurations.

Soldati and Marchioli [7] examine state-of-the-art Direct Numerical Simulations (DNS) and Large Eddy Simulations (LES) applications of Lagrangian particle tracking of sediment transport in steady turbulent boundary layers. Kidanemariam and Uhlmann [8] use an immersed boundary approach to simulate pattern formation on a sediment bed. Schmeekle [9] simulates turbulent flow over a backward-facing step with a LES approach, coupled to a discrete element method (DEM), to investigate the interaction between bed load transport and turbulent separated flow. Escauriaza and Sotiropoulos [10] use a detached eddy simulation (DES) and LPT to provide insights into the initiation of particle motion and bed-load flux of flow over a particle bed and past a vertical cylinder. They conducted similar simulations using an Eulerian sediment model [11] to produce ripple dynamics seen in laboratory experiments and nature. Link et al. [12] utilize the LPT method of Escauriaza and Sotiropoulos [10] and DES to study a similar configuration using laboratory results to simulate the flow field. Modeling the sediment with an Eulerian approach, Chou and Fringer [13] simulate bed form evolution by non-equilibrium turbulent flows. Yu et al. [14] find noticeable turbulence damping by the presence of sediment using a DNS-Eulerian approach whereby the only coupling of the fluid and solid phases is done through a particle-induced fluid density modification. Khosronejad and Sotiropoulos [15] use an IB to model the fluid-solid interface and unsteady Reynolds-average Navier Stokes method to study flow over a bed and around varying pier shapes.

The present study is the investigation of the interactions between coherent structures and an erodible surface, here a sediment bed. We chose to reduce the problem to the simplest model of coherent structures that mimics wall turbulence: the vortex pair. The vortex pair is representative of many fundamental flow structures, such as quasi-streamwise vortices found in turbulent flow, and trailing vortices arising from flow over bluff bodies. In this work, the vortex pair is a 2D vortex dipole. Orlandi [16] was the first to conduct a numerical simulation of a vortex dipole rebound from a wall. A broad review of vortex-wall interactions is given by Doligalski et al. [17]. Another motivation comes from the recent works of Sano et al. [18] and Munro [19], who have conducted experiments in which a vortex ring collides with an erodible sediment bed. Munro [19] measured the deformation of the sediment bed for a range of vortex ring impulse strengths, and sediment particle sizes and densities. Using a variety of vortex ring strengths and initial distances from the particle bed, Masuda et al. [20] and Yoshida [21] explained the scour pattern regimes associated with particular Reynolds number ranges and initial distances. In the spirit of investigating the evolution of the interactions between coherent structures and the erodible surface, we focus our study on repeated impacts of vortex pairs on a sediment bed. This particular scenario is intended to mimic repetitive phenomena

such as quasi-periodic vortex separation or vortices arising from periodic flow rates (e.g. tides). The authors recognized that the absence of shear flow (simulations are confined to 2D) limit the practical application of the simulation. This study should be seen as a first step in a new area of research: the evolution of scour under repeated erosion events. Future studies will likely include variation of the strength of erosion events in three dimensional flows. In the following, the governing equations and numerical method are first briefly summarized, followed by a description of the numerical simulation configuration and set up. The scour characteristics and flow dynamics are then analyzed. Finally, some concluding remarks are presented.

The direct numerical simulations discussed in this paper use a finite volume approach detailed in [22], and are both two and three dimensional. The particles modeling the sediment bed are resolved through a Discrete Particle Model (DPM). The DPM treats the fluid as a continuum and the particles as distinct entities. The model is four-way coupled, whereby the fluid feels the effects of each particle, each particle feels the effect of the surrounding fluid, and particle-particle interactions (here collision) are accounted for. The model was pioneered by Cundall and Strack [23]. Zhu et al. [24, 25] review the theoretical developments of the method and provide a summary of DPM applications and findings. The details of the model are summarized in Section 2, following the application by Capecelatro and Desjardins [26], [27], [28] and Pepiot and Desjardins [29]. The DPM has many applications, including fluidized beds (see the review of DPM application to fluidized beds by Deen et al. [30]) and other particle-fluid flows. However, there has been limited application to the study of scour. Zamankhan [31] used LES and DPM to simulate 3D flow over a pipeline, and found good agreement with experimental results.

2. Governing Equations & Numerical Methodology

The gas/fluid phase is governed by the Low Mach Approximation incompressible Navier-Stokes equations, and the solid phase particles are described by the Discrete Particle Model (DPM), or Lagrangian Particle Tracking (LPT) method, as described by Capecelatro and Desjardins [26] and Pepiot and Desjardins [29]. These equations are implemented in an arbitrarily high-order, massively parallel numerical code capable of direct numerical simulations (DNS), described by Desjardins et al. [32]. This code is staggered in both space and time, and, in this work, spatial and temporal integrations are second-order accurate. The scheme conserves mass, momentum, and energy. Time advancement is done using a fractional step Crank-Nicolson scheme. For the full details, the reader is referred to Desjardins et al. [32] and Pepiot and Desjardins [29]. The following serves as an overview of their methodology.

Taking into account the volume occupied by the particles, the continuity equation is

$$\frac{\partial}{\partial t}\left(\psi_f \rho_f\right) + \nabla \cdot \left(\psi_f \rho_f \mathbf{u}_f\right) = 0, \tag{1}$$

where ψ_f is the volume fraction of the fluid, ρ_f is the density of the fluid, and $\mathbf{u}_f$ is the velocity of the fluid. With the addition of a source term for the exchange of momentum with the solid phase, $\mathbf{F}_{inter}$, the conservation of momentum equation becomes

$$\frac{\partial}{\partial t}\left(\psi_f \rho_f \mathbf{u}_f\right) + \nabla \cdot \left(\psi_f \rho_f \mathbf{u}_f \mathbf{u}_f\right) = \nabla \cdot \tau + \mathbf{F}_{gravity} - \mathbf{F}_{inter}. \tag{2}$$

Where $\mathbf{F}_{gravity} = \psi_f \rho_f \mathbf{g}$, and τ is the stress tensor

$$\tau = -p\mathbf{I} + \mu\left(\nabla \mathbf{u}_f + \nabla \mathbf{u}_f^T\right) - \frac{2}{3}\mu \nabla \cdot \mathbf{u}_f \mathbf{I}. \tag{3}$$

The pressure is denoted by p, $\mathbf{I}$ is the identity matrix, and μ is the dynamic viscosity.

The solid phase is tracked in a Lagrangian framework, so that the location of an individual particle is defined by

$$\frac{d\mathbf{x}_p}{dt} = \mathbf{u}_p. \tag{4}$$

According to Newton's second law of motion, particles are governed by

$$m_p \frac{d}{dt}\left(\mathbf{u}_p\right) = \mathbf{f}_{inter} + \mathbf{F}_{col} + m_p \mathbf{g}, \tag{5}$$

where m_p is the mass of the particle, $\mathbf{u}_p$ is the velocity of the particle, $\mathbf{f}_{inter}$ is the exchange of momentum with the fluid for the single particle, and $\mathbf{F}_{col}$ is the force imparted by collisions with other particles or a wall. For a given cell volume, the sum of all of the single particle momentum exchanges, $\mathbf{f}_{inter}$, gives the full momentum exchange term in Equation 2

$$\mathbf{F}_{inter} = \sum_{i}^{N_p} \mathbf{f}_{inter}^i. \tag{6}$$

The collision term, $\mathbf{F}_{col}$, represents the sum of the all collision forces acting on a given particle. The momentum exchange between the fluid and solid phases is contained within this term and its application in Equations 2 and 5.

3. Vortex Dipole

In this work, the vortex-dipole is based on the Lamb-Oseen vortex:

$$V_\Theta(r) = \frac{\Gamma}{2\pi r}\left(1 - \exp\left[\frac{-r^2}{r_c^2}\right]\right) \tag{7}$$

Γ is the circulation, r is the radial distance from the center of the vortex, and r_{core}, or r_c, is the radius from the vortex center to its core, at which the circumferential velocity, V_Θ, is a maximum. A cross section of the velocity profile of the Lamb-Oseen vortex can be seen in Figure 1(a). Only at significant distances from the center of the vortex does the vortex field become negligible. Even at $r/r_c = 50$, the velocity is still over 3% of the maximum V_Θ.

The vortex-dipole is created by combining two lamb-oseen vortices of opposing orientation. Each Lamb-Oseen vortex is shifted an equal distance, x_c, from the center of the domain. With the radial distance, $r = \sqrt{(x \pm x_c)^2 + (y \pm y_c)^2}$, and $y_c = 0$, the shifted Lamb-Oseen vortex flow field equations become:

$$V_\Theta(r) = \pm\frac{\Gamma}{2\pi\sqrt{(x \mp x_c)^2 + y^2}}\left(1 - \exp\left[-\frac{(x \mp x_c)^2 + y^2)}{r_c^2}\right]\right) \tag{8}$$

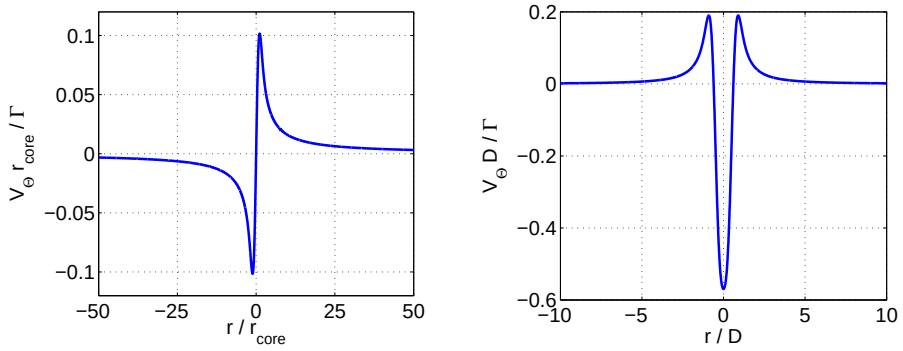

(a) Lamb-Oseen Vortex (b) Vortex Dipole

Figure 1. (a) Lamb-Oseen vortex velocity profiile cross section. Single vortex centered in domain, spinning counter-clockwise. The maximum velocity occurs at $r = r_{core}$. (b) Vortex-dipole velocity profile cross section. At the center of dipole, the velocity fields amplify, and the net effect is the self-induced downward motion of the dipole.

And the vortex-dipole equation is simply the sum of these two equation:

$$V_\Theta(r) = \frac{\Gamma}{2\pi\sqrt{(x-x_c)^2+y^2}}\left(1-\exp\left[-\frac{(x-x_c)^2+y^2}{r_c^2}\right]\right) - \frac{\Gamma}{2\pi\sqrt{(x+x_c)^2+y^2}}\left(1-\exp\left[-\frac{(x+x_c)^2+y^2}{r_c^2}\right]\right) \tag{9}$$

A cross-section of the velocity profile of the vortex-dipole is shown in Figure 1(b). The parameters of the dipole are configured based on the work by Kravchenko et al. [33]. The statistically averaged distance between streamwise vortices in a turbulent channel flow is roughly three times the core radii of the streamwise vortices. Therefore, the core radius of each vortex of the dipole is $r_c = \frac{1}{3}D$, where D is the diameter of the dipole. The dipole velocity field decays much more rapidly than the velocity field of a solitary vortex. This is due to the opposing orientations of the two vortices, which amplify at the center of the domain, but damp elsewhere. In isolation, each vortex has zero velocity at its center, and would simply rotate without any translative motion. However, when the velocity fields of the two vortices are combined to form the dipole, the velocity component from one vortex, calculated at the location of the center of the other vortex, is purely downward. Therefore, the dipole propagates downwards toward the wall.

In the process of validating their high order conservative finite difference scheme, Desjardins et al. [32] conducted numerous test cases. Included in these case were the propagation of a vortex dipole and the collision of a vortex ring on a wall, both showing good agreement with the results of Verzicco and Orlandi [34].

4. Simulation Configuration & Methodology

This work is comprised of two sets of simulations. One set is purely two-dimensional (2D), the other is "quasi-2D". The quasi-2D simulations use the same configuration as the purely 2D simulations, except the third dimension has been slightly expanded to account for the three-dimensional effects of the spherical particles. In the quasi-2D case, the 2D vortex-dipole is expanded, creating a pair of cylindrical vortices. Figure 2 presents a schematic of the initial configuration of the simulation. There are 256 wall-parallel nodes and 150 wall-normal nodes. The wall at the bottom of

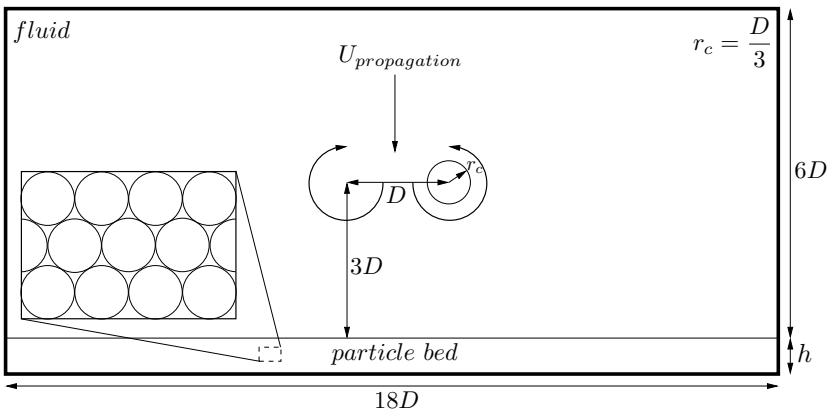

Figure 2. Initial configuration of the simulation. The vortex dipole is centered in the domain, starting $3D$ from the particle bed. The core of each vortex is located at a distance $r_c = D/3$ from vortex centers. The bed is comprised of particles in a tightly packed formation to a height of h.

the domain has a no-slip boundary condition and is covered by a bed of particles, held in place by the gravitational force, acting downward, towards the wall. The particle bed comprises 30 layers of tightly packed particles, per Figure 2, resulting in 27,000 total particles, and a settled bed height $h \simeq 25d_p$. In the quasi-2D case, the third dimension is expanded with 4 nodes, or 10 particle diameters, resulting in total 270,000 particles in the bed. The domain is periodic in both wall-parallel directions.

To conduct the study of the repeated impacts of the vortex dipole onto the particle bed, the following methodology is followed.

(1) Due to the nature of the soft-sphere collision model, and despite building the particle bed so that the particles are closely packed, the bed must settle under the effect of gravity. In order to make sure that this process is isolated from any erosive behavior caused by the vortex dipole, the bed must be allowed to settle under the effect of gravity alone. Therefore, the full simulation domain is initialized with a zero velocity field. The particles then settle into an equilibrium state with the effect of gravity and the bottom wall. Since the bed is initialized in a close-packed structure, the settling process only slightly compresses the particles, but does not cause reshuffling. The final, settled, particle bed is stable and level.
(2) Once the particle bed has settled, the vortex dipole is initialized and collides with the settled, and non-scoured, particle bed. The vortices either entrain the particles into the fluid or force them to slide and/or roll on top of one another. The simulation is run until all of the particles have been re-deposited to the surface by the gravitational force and the vortices dissipate (ensuring that further erosion will not occur). The evolution of a typical system is illustrated in Figure 3.
(3) The newly scoured bed is retained and the flow field is reset to that of the original vortex dipole. This second dipole impacts the scoured bed. Again, the particles are allowed to settle and the vortices to dissipate.
(4) Step 3 is repeated.

Steps 1-4 are repeated for a range of Shields parameters, where the Shields parameter is the ratio of disturbing forces to restorative forces. In this case, those are the fluid shear stress at the bed, $\tau_{bed} = \frac{\mu \partial u}{\partial y}$, and gravity, respectively. The Shields parameter is then $\Theta = \tau_{bed}/(\rho_p - \rho_f)gd$. The densities of the solid and fluid phases are ρ_p and ρ_f, respectively and the particle diameter d is $1000\,\mu m$. The critical value of the Shields parameter, Θ_c, is the threshold beyond which incipient bed

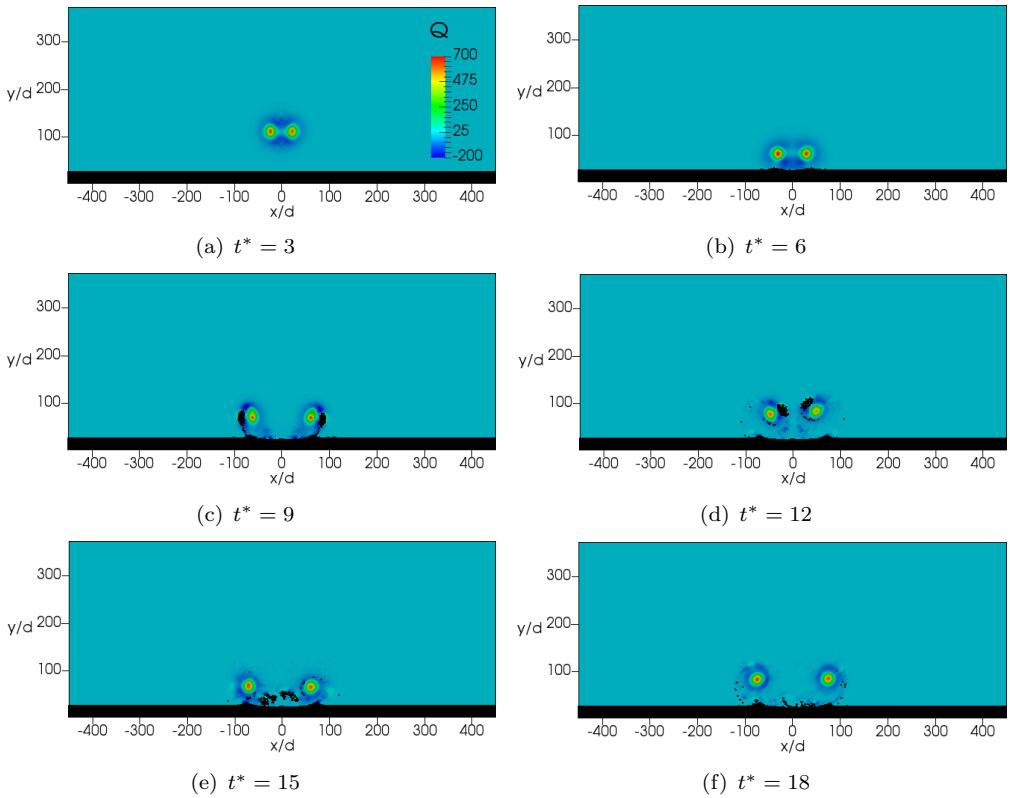

(a) $t^* = 3$ (b) $t^* = 6$

(c) $t^* = 9$ (d) $t^* = 12$

(e) $t^* = 15$ (f) $t^* = 18$

Figure 3. The purely 2D vortex dipole propagates downward until it impacts the particle bed. Time is normalized by the initial diameter of the vortex dipole and the initial propagation velocity of the vortex dipole, so that $t^* = t * u_{0,propagation}/D$. Much like a vortex dipole impacting a no-slip wall, the vortices rebound, but since the wall is a particle bed in this case, particles are entrained by the fluid. The effect of gravity pulls the entrained particles back to the bed, the vortices eventually separate and dissipate, and a scoured bed topography is left. The Shields number is $\Theta/\Theta_c = 4.5$.

Table 1. The Shields number is modified by changing the particle density, ρ_p. At the critical Shields number, $\Theta/\Theta_c = 1$, the particle density is 1900 kg/m^3 (highlighted in bold).

ρ_p $[kg/m^3]$	2500	2200	**1900**	1600	1300	1200	1100
Θ/Θ_c	0.6	0.75	**1**	1.5	3	4.5	9

particle motion is observed. In the purely 2D cases, the repeated impacts were conducted at Θ/Θ_c of 1, 1.5, 3, and 4.5. In the quasi-2D case, the repeated impacts are conducted at Θ/Θ_c of 9. Munro et al. [19] used relative Shields numbers, Θ/Θ_c, in the range of 1 through 10 to achieve their scour patterns. The Reynolds number of the vortex dipole is defined as $Re_U = u_{0,propagation}D/\nu$, where $u_{0,propagation}$ is the propagation velocity of the dipole, D is the dipole diameter, and ν is the kinematic viscosity of the fluid. (It should be noted that the dipole diameter $D = 50d_p$.) All simulations were conducted with a Reynolds number of 5600, which is right in the middle of the range used by Munro et al. [19] in their experiments. Both gravity, $g = -9.81\,m/s^2$, and the particle diameter, $d = 1000\,\mu m$, are constants. Therefore, in order to alter Θ, the particle density is modified, per Table 1. A standard assumption of sediment density is roughly 2700 kg/m^3. However, in order to utilize a lower Reynolds number flow, and thus larger grid spacing, lower densities were required.

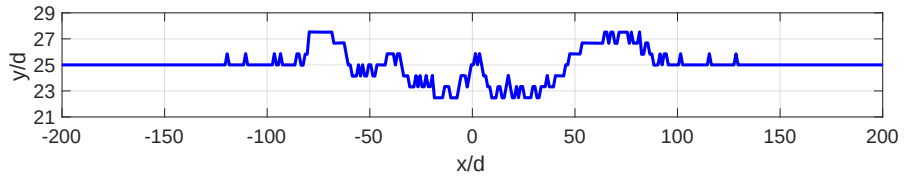

(a) 2D Topography

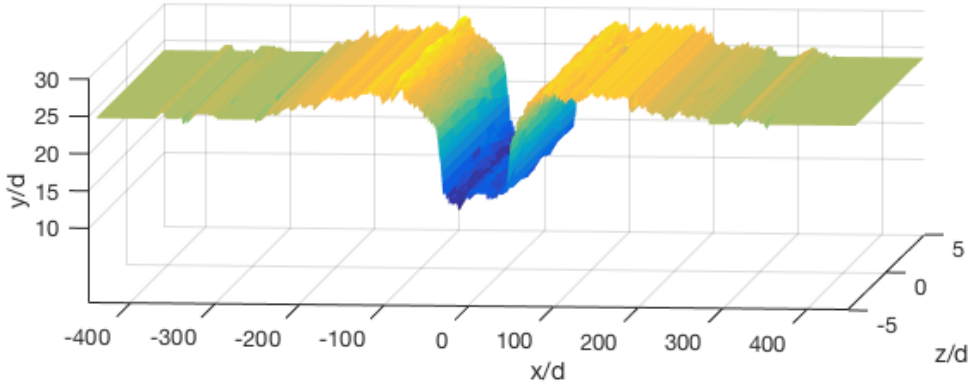

(b) Quasi-2D Topography

Figure 4. Scour topographies resulting from the impact of the initial vortex dipoles. All dimensions are normalized by the particle diameter. (a) Purely 2D at a Shields number of $\Theta/\Theta_c = 3$. (b) Quasi-2D case at a Shields number of $\Theta/\Theta_c = 9$.

5. Results

5.1. *Scour Hole Characteristics*

The observed scour hole topography resulting from the impact of the initial vortex dipole displays universal characteristics at all Shields numbers. At Shields numbers above the critical value, some particles become entrained in the fluid of the vortex and are swept away from the bed. Particles that are near the impact zone, but are not entrained, are swept to each side of the scour hole, forming mounds. This process is shown in Figure 3 for $\Theta/\Theta_c = 4.5$. The impacts of the initial dipole yield a somewhat universal surface topography, whereby each vortex sweeps away a "u" shape, resulting in a "w" shape overall. The scour hole displays a local maximum, or peak, at the center of the hole, and a mound is formed on each side of the hole. Even at the critical Shields number, where incipient particle motion is observed, and below which no particles are dislodged, this phenomena is observed, albeit at a smaller scale. Because the relative effect of the gravitational force is so strong, the vortex dipole manages to push only a few particles up and over their neighbors, but the particles never become entrained in the fluid. The maximum scour hole depth is generally observed directly below either of the vortices in the dipole, where the shear bed stress is at a maximum. At higher Shields numbers, the entrained particles may fall back into the scour hole. Therefore, the scour hole shape is not necessarily smooth. It should also be noted that below the critical Shields number, slight particle oscillation about their original positions may be observed, but ultimately these particles are not dislodged from their original positions. The scour hole topographies for the purely 2D case and the quasi-2D case are shown in Figure 4.

The bed shear stress at the fluid-bed interface is shown in Figure 5(a), for the first vortex dipole impact at $\Theta/\Theta_c = 4.5$. At time $t^* = t * u_{0,propagation}/D \simeq 4$, just as the dipole begins to impact the wall, bed shear maximums are found below each

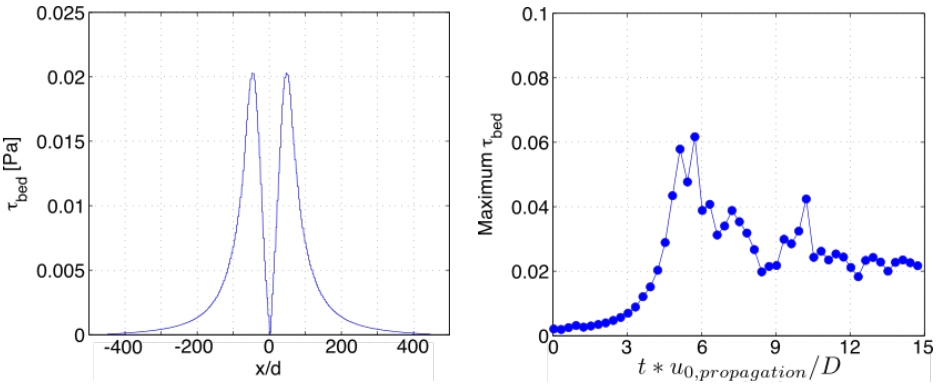

(a) Bed shear stress (b) Maximum bed shear stress

Figure 5. (a) Bed shear stress, τ_{bed}, at non-dimensional time $t^* \simeq 5$, $\Theta/\Theta_c = 4.5$. The two maxima correspond to the two vortices that comprise the dipole. τ_{bed} decays to zero as the distance from the vortex dipole centerline increases. τ_{bed} also goes to zero at the dipole centerline, since the symmetry of the flow eliminates any horizontal velocity component at this location, and vertical velocity components are zero at the wall. (b) Maximum bed shear stress.

vortex of the dipole, with the bed shear stress decaying to zero towards the edges of the domain. Figure 5(b) shows the maximum bed shear stress over time. The first peak, at time $t^* \simeq 5.5$, occurs when the vortex dipole interacts with the bed the first time. The second smaller peak, at time $t^* \simeq 10$, occurs after the individual vortices rebound from the wall, move back toward their original centerline, and interact with the bed for a second time.

The evolution of the scour hole topography with successive impacts is shown in Figure 6. At the critical Shields number, the maximum scour hole depth is not significantly altered with subsequent impacts of the vortex dipole. The characteristic removal of particles at the points of impact, and the formation of mounds to each side of the scour hole are observed to only be a single particle diameter in magnitude in this case. At higher Shields numbers, $\Theta/\Theta_c = 3$ and $\Theta/\Theta_c = 4.5$, the first two impacts display the characteristic scour hole pattern of the lower Shields number simulations, but with greater magnitude. Figures 6(c) and 6(d) show much more exaggerated scour hole depths, small local peaks within the holes, and mounds to the sides of the holes. By the third impacts, however, the small local peaks in the scour hole are no longer observed. Figure 6(e) shows the evolution of the scour hole in the quasi-2D case. It is clear that the majority of the scour hole depth is achieved by the first impact. Subsequent impacts do not drastically alter the shape or the maximum depth of hole.

The evolution of the scour hole topographies reveal two scour hole depth regimes. In the first scour regime, the maximum depth of the scour hole changes with each impact of the vortex dipole. In the second scour regime, the impacts of vortex dipoles continue to modify the topography of the bed, but the maximum scour hole depth is unchanged. In this work, the scour hole depth is defined as the distance between the lowest point of the fluid-bed interface and the original height of the bed, $y = h$. As shown in Figure 7(a), the first regime is composed of the initial, or first few, impacts, depending on Shields number. In this regime, the maximum scour hole depth, h, increases with subsequent impacts of the vortex dipole. However, after a finite number of impacts, the scour hole depth is approaching, or has reached, its asymptotic limit, which is the second regime. In the second regime, additional impacts may alter the scour topography, but the scour hole depth does not oscillate by more than a particle diameter above or below a maximum scour hole depth. This particular phenomenon can be seen at the two highest Shields

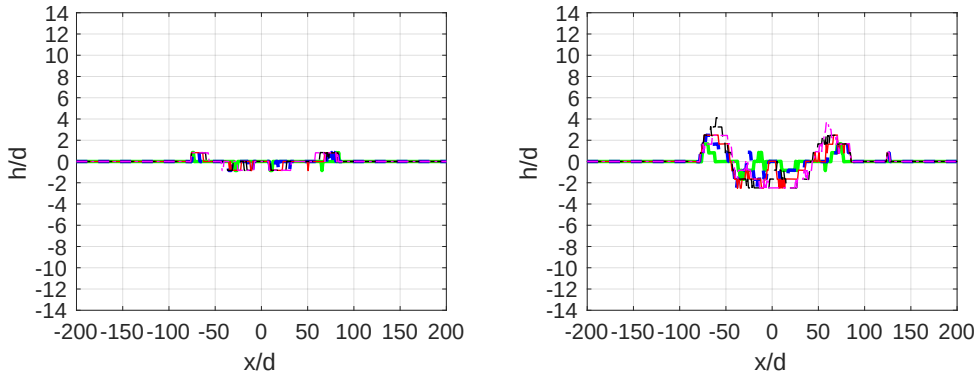

(a) 2D $\Theta/\Theta_c = 1$

(b) 2D $\Theta/\Theta_c = 1.5$

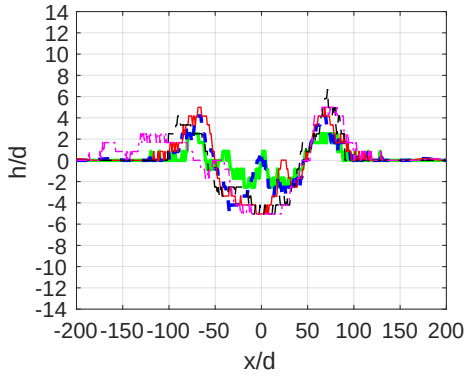

(c) 2D $\Theta/\Theta_c = 3$

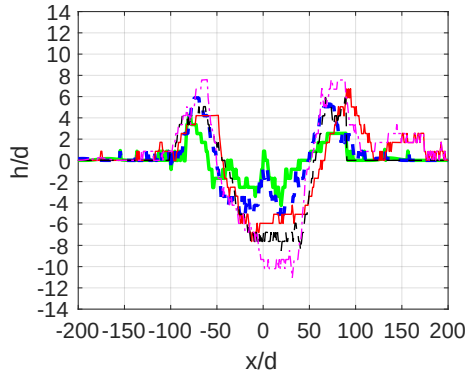

(d) 2D $\Theta/\Theta_c = 4.5$

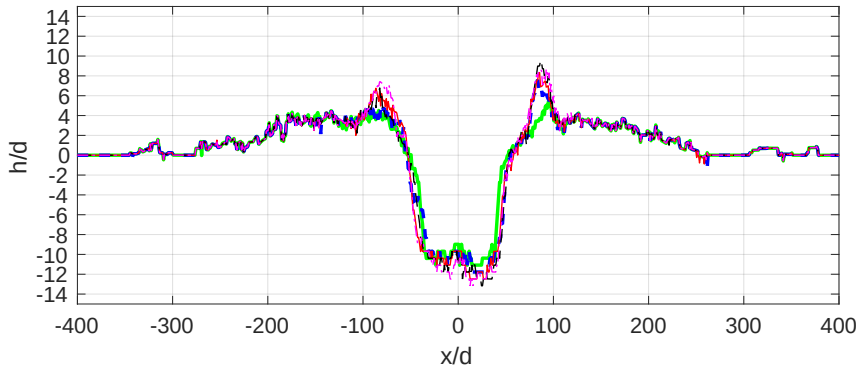

(e) Quasi-2D $\Theta/\Theta_c = 9$

Figure 6. Scour hole topography for the range of Shields numbers examined. All dimensions are normalized by the particle diameter. The succession of impacts is denoted as follows (color in online version only): 1^{st} (———, green), 2^{nd} (– – – –, blue), 3^{rd} (———, red), 4^{th} (– – – –, black), 5^{th} (– · –, magenta). (a) At the critical Shields number, the flow is only able force a few particles to slide over neighboring particles. (b)-(d) At higher numbers, the characteristic "w" scour hole shape is created by the first impacts. The eroded particles are forced into mounds, or peaks, which surround the scour hole. (e) Quasi-2D simulation at the highest Shields number clearly shows the characteristic scour hole shape. Also note that the initial impact does the majority of the scouring.

numbers. For the critical Shields number, the initial impact determines the final scour hole depth (regime 1), regardless of how many subsequent impacts (regime 2) on the bed are made. For Θ/Θ_c of 1.5, and 3, the maximum scour hole depth is achieved by the second impact (regime 1), and no increase in the scour hole depth is seen with further impacts (regime 2). At Θ/Θ_c of 4.5 and 9, more impacts are required to achieve the maximum scour hole depth asymptotic limit. At $\Theta/\Theta_c = 4.5$,

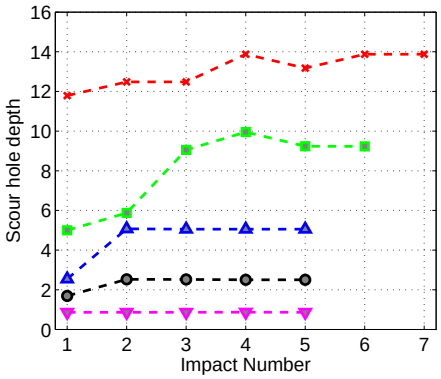

(a) Maximum scour hole depth, h

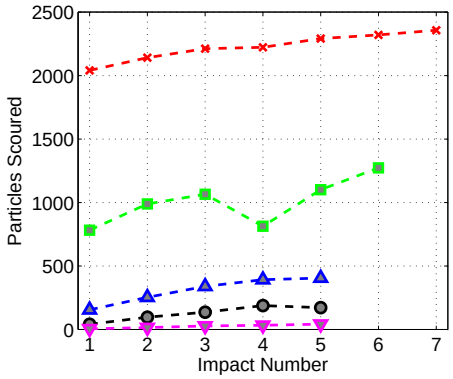

(b) Number of scoured particles

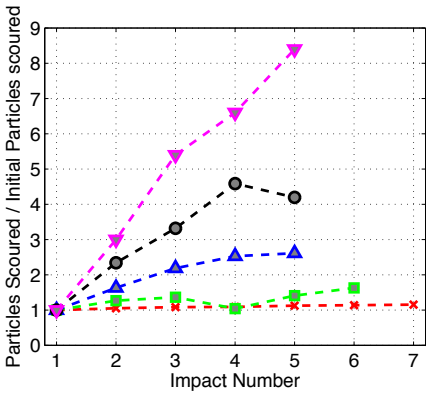

(c) Number of scoured particles

Figure 7. (a) Scour hole depth h, normalized by the particle diameter. Five impacts are displayed: $\Theta/\Theta_c = 1$ ($\triangledown$), $\Theta/\Theta_c = 1.5$ ($\circ$), $\Theta/\Theta_c = 3$ ($\triangle$), $\Theta/\Theta_c = 4.5$ ($\square$), $\Theta/\Theta_c = 9$ ($\star$). (b) Total number of scoured particles. (c) Total number of scoured particles, normalized by the particle diameter and the number of particles scoured during the initial impact for each Shields number.

regime 1 consists of the first three impacts, and all subsequent impacts fall into regime 2. At $\Theta/\Theta_c = 9$, the first four impacts make up regime 1, and regime 2 is comprised of all subsequent impacts.

In scour regime two, the scouring processes continue to modify the bed topology even though the scour hole depth has reached its asymptotic maximum. In this work, a particle is determined to be "scoured" if it has been moved from below the original height of the bed, where $y = h$, to above it. So, even if a particle has been displaced from its original location, it is not defined as scoured if it remains within the scour hole and below the original height of the bed. The purpose of this definition is meant only to help define the characteristics of the scoured fluid-bed interface topology, not to exactly describe the motion of individual particles. The total number of scoured particles are shown in Figures 7(b). At the lowest Shields number, the maximum scour hole depth does not change after the first impact. And yet, the number of particles scoured increases with subsequent impacts. As was shown in Figures 6(a) and 7(c), at the critical Shields number, the first impact only displaces a handful of surface particles. As the vortices continue to impact the bed, the scour hole retains its depth of a single particle diameter, but becomes wider with each subsequent impact. At higher Shields numbers, more impacts are required to reach scour regime 2, but the percentage of total scoured particles does not change as drastically. As the Shields parameter increases, the first impact scours a higher and higher percentage of total particles scoured, per Figure 7(c).

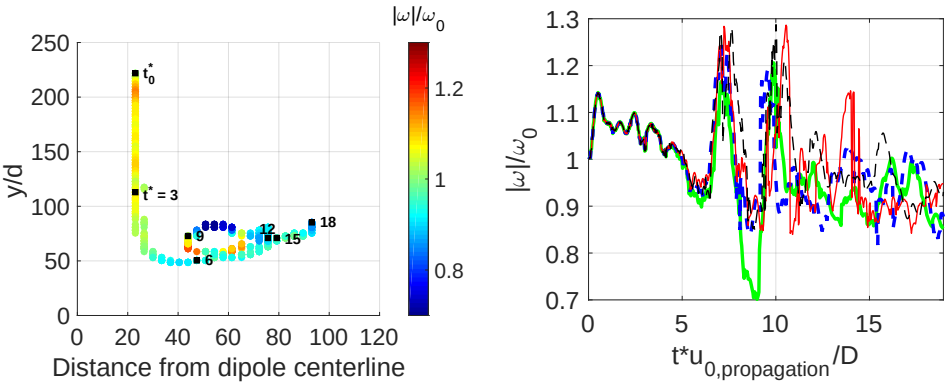

(a) (b)

Figure 8. $\Theta/\Theta_c = 4.5$. (a) Vortex core path of first impact. The vorticity is normalized by the initial vorticity value. Time is normalized by the initial diameter of the vortex dipole and the initial convection velocity of the vortex dipole, and denoted as $t^* = t*u_{0,propagation}/D$. All other dimensions are normalized by the particle diameter. The vortex core locations are colored by the vorticity of the vortex. (b) Evolution of the normalized vorticity, for all five impacts. The impact numbers are (color online only): 1^{st} (———, green), 2^{nd} (– – – –, blue), 3^{rd} (———, red), 4^{th} (– – – –, black), 5^{th} (– · –, magenta).

5.2. *Flow Dynamics*

Per Lim et al. [35], when a vortex dipole impacts a solid wall, the two vortices spread apart at impact, rebound from the wall, then moves back towards toward the centerline and toward the wall a second time before dissipating. Although the fluid-bed interface in this work does not have a no-slip condition since the particles in the bed are mobile, the vortex cores display the same general behavior observed by Lim. Figure 8(a) plots the path of the vortex center for the first impact at $\Theta/\Theta_c = 4.5$, where the center location is colored by the vorticity. The vortex interacts with the bed at $t^* = t * u_{0,propagation}/D \simeq 6$, then again at $t^* \simeq 11$. In between the two interactions, the vortex moves away from the bed and back toward the centerline, the path looping back over itself. At $t^* > 12$, the vortex repeats the looping motion, but at much smaller scales, and further from the bed, before dissipating. The vorticity shown in Figure 8(a) is plotted over time in Figure 8(b), along with the evolution of vorticity for the subsequent impacts. The two main bed interactions, at times $t^* \simeq 6$ and $t^* \simeq 11$ manifest as local minima in the evolution of the vorticity. The global vorticity minimum at $t^* \simeq 9$, is observed when the vortex moves away from the bed in between the first and second interactions with the bed. Bookending this global minimum are the two global maxima peaks, at $t^* \simeq 7$ and $t^* =\simeq 10$. Vorticity production at a wall has been observed by Kramer et al. [36]. Kramer et al. found that vorticity can be produced locally at a no-slip boundary. In this work, the boundary is the fluid-bed interface of the particle bed, which is not strictly no-slip, but has proven capable of sustaining sufficient stress for vorticity production.

As the topography of the particle bed changes with repeated impacts, the paths of the vortex dipoles change as well. At lower Shields parameters, less scouring results in smaller changes to the fluid-bed interface, which in turn, means smaller changes to the paths of the vortices that interact with them. At higher Shields parameters, larger scale scouring and fluid-bed interface modification result in larger changes in vortex core paths. In Figure 9, examples of two different types of vortex center evolutions are shown. At $\Theta/\Theta_c = 1$, the maximum scoured depth, in combination with the height of the resulting particle mounds, are on the order of a single particle diameter. So, the topology of the fluid-bed interface is not significantly altered by the repeated impacts. Therefore, the paths of the vortices that impact these

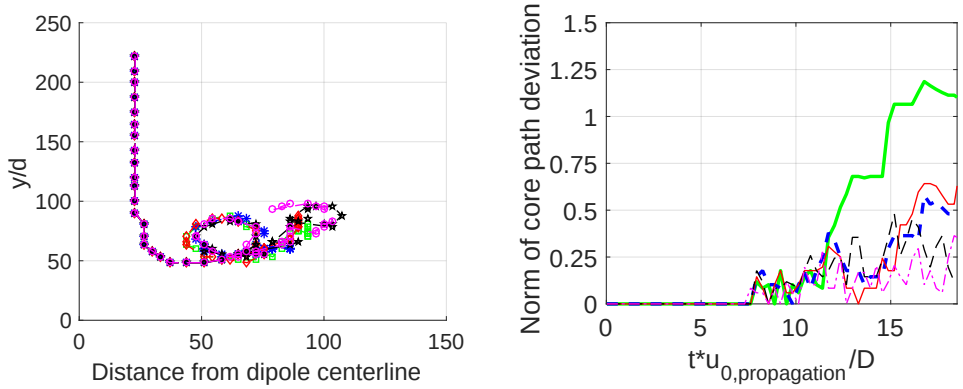

(a) $\Theta/\Theta_c = 1$ (b) $\Theta/\Theta_c = 1$

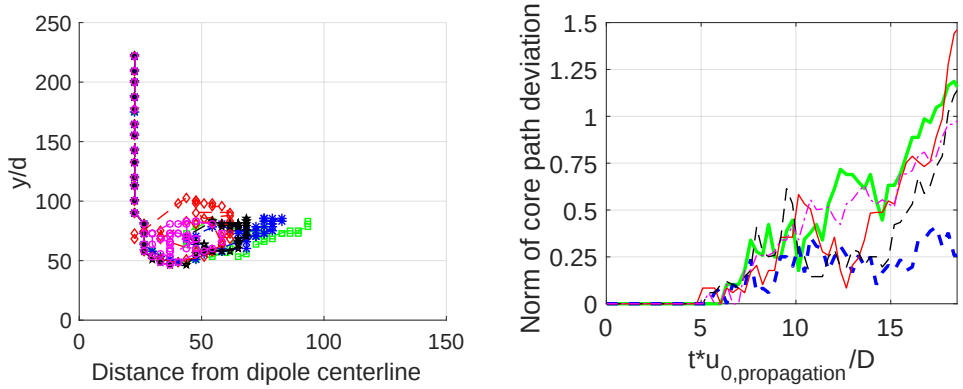

(c) $\Theta/\Theta_c = 4.5$ (d) $\Theta/\Theta_c = 4.5$

Figure 9. Vortex trajectories for the first five impacts are shown in (a) and (c). All dimensions are normalized by the particle diameter. The impact number is indicated by the color of the line: 1^{st} ($\square$, green), 2^{nd} ($*$, blue), 3^{rd} ($\diamond$, red), 4^{th} ($\star$, black), 5^{th} ($\circ$, magenta). The deviations of the vortex trajectory from the vortex trajectory of the previous impact are shown in (b) and (d). The deviation is normalized by the initial diameter of the vortex dipole, D. The impact numbers are (color online only): 1^{st} (———, green), 2^{nd} (- - - -, blue), 3^{rd} (———, red), 4^{th} (- - - -, black), 5^{th} (– · –, magenta). Subsequent impacts are compared to the previous impact (i.e. The second impact is compared to the first impact, the third impact is compared to the second impact, etc. The first impact is compared to the trajectory of a vortex impacting a wall at sub-critical $\Theta < \Theta_c$, where no scouring occurs).

scoured beds are not significantly altered either. In Figure 9(a), the vortex center paths display the same general behavior, looping away from the wall and back toward the centerline, before moving away from the bed and dissipating. Figure 9(b) quantifies this as the deviation of the vortex path, defined as the norm of the difference between the path of the current path and the path of the previous impact. (The deviation of the vortex center path of the first impact is compared to the path of a sub-critical Shields number impact, where no scouring occurs.) In fact, the deviation of the vortex paths decrease with each subsequent impact. By the final impact, the norm of the vortex core path deviation stays under 25% even after the vortex core's second interaction with the fluid-bed interface.

At the highest Shields numbers, after the second impact, the magnitude of the scour hole depth, on the order of ten particle diameters, is sufficient to constrain the paths of the vortex cores. This is an order of magnitude greater than the scour hole depth at the lowest Shields parameters. At $\Theta/\Theta_c = 4.5$, as shown in Figure 9(c), the trajectories of the third, fourth, and fifth impact vortices do loop upon themselves but do not then drift away from the original dipole centerline. Instead, they loops back towards the centerline again and remain in this pocket of the scour hole. In 9(d), the vortex path from the second impact shows a marked drop in

path deviation, much like in 9(b). However, the vortex paths from the third, fourth and fifth impacts do not follow this trend, displaying path deviations similar to that of the very first impact. For all Shields numbers, vortex containment by the combination of the scour hole depth and corresponding mounds, h_{total}, was first observed when $h_{total} > 5$ particle diameters, or $h_{total} > 0.1D$, ten percent of the original dipole diameter.

6. Conclusion

We investigated the evolution of scour under repeated impacts of a vortex pair on a sediment bed at different Shields numbers. Two sets of numerical simulations were conducted. A set of purely two dimensional simulations, and separate quasi two dimensional simulations. All simulations use an Euler-Lagrange approach called the Discrete Particle Method (DPM), where particles are four-way coupled. The DPM has been shown to be a good tool to investigate the interaction between flow dynamics and particles. In this work, a particle bed is subjected to a series of impacts by a vortex dipole. In the purely 2D case, a Shields number parameter space ranging from the critical value (below which, no scouring occurs) to 4.5 times the critical value was used. In the quasi-2D case, a Shields number 9 times the critical value was used.

The scour topographies show a universality for all Shields numbers, particularly after the initial impacts. At all Shields numbers, the vortex dipole penetrates the surface of the particle bed, each vortex of the dipole scouring the particles directly underneath and sweeping them away from the centerline of the dipole. The result is a scour topography comprised of a w-shaped hole with a small, local peak at the center and a mound of particles to each side of the hole. This topography is observed at all Shields numbers after the first impact, but the small local maximum may be erased by subsequent impacts. At higher Shields numbers, the magnitude of the scour hole characteristics become large enough to significantly alter the behavior of the vortex dipole. As the magnitude of the scour hole depth and the height of the particle mounds to each side of the hole become larger, the vortex dipole is trapped by the particle mounds. For the flow configuration of this work, the critical combined distance between the bottom of the scour hole and the top of the mounds was found to be $h_{critical} \simeq 0.1D$, which resulted in modified vortex trajectories. No matter the scouring mechanism, for all Shields numbers, the maximum scour hole depth eventually reached an asymptotic limit, past which, further impacts did not increase the maximum scour hole depth. At the two highest Shields numbers, once the asymptotic limit was reached, subsequent impacts can increase or decrease the depth by a particle diameter, but further impacts showed that this was a fluctuation, not a fundamental change in the scour hole depth.

Acknowledgments

This work was supported (in part) by the USDOT through the UTC program at the University of Vermont. The efforts of D. Hagan and Y. Dubief on this work were also partially supported by NSF CBET-0967224 and NASA NNX11AM07A.

References

36

[1] H. Breusers, and A.J. Raudkivi *Scouring: Hydraulic Structures Design Manual Series, Vol. 2*, AA Balkema Rotterdam,, The Netherlands, 1991.

[2] G. Hoffmans, and H. Verheij *Scour manual*, Balkema Rotterdam, The Netherlands, 1997.

[3] B.W. Melville, and S.E. Coleman *Bridge scour*, Water Resources Publication, 2000.

[4] G.J. Hoffmans *The influence of turbulence on soil erosion*, Vol. 10, Eburon Uitgeverij BV, 2012.

[5] B. Mutlu Sumer, *Mathematical modelling of scour: A review*, Journal of Hydraulic Research 45 (2007), pp. 723–735.

[6] J. Jiménez, and A. Pinelli, *The autonomous cycle of near-wall turbulence*, Journal of Fluid Mechanics 389 (1999), pp. 335–359.

[7] A. Soldati, and C. Marchioli, *Sediment transport in steady turbulent boundary layers: Potentials, limitations, and perspectives for Lagrangian tracking in DNS and LES*, Advances in Water Resources 48 (2012), pp. 18–30.

[8] A.G. Kidanemariam, C. Chan-Braun, T. Doychev, and M. Uhlmann, *Direct numerical simulation of horizontal open channel flow with finite-size, heavy particles at low solid volume fraction*, New Journal of Physics 15 (2013), p. 025031.

[9] M.W. Schmeeckle, *The role of velocity, pressure, and bed stress fluctuations in bed load transport over bed forms: numerical simulation downstream of a backward-facing step*, Earth Surface Dynamics Discussions 2 (2014), pp. 715–732.

[10] C. Escauriaza, and F. Sotiropoulos, *Lagrangian model of bed-load transport in turbulent junction flows*, Journal of Fluid Mechanics 666 (2011), pp. 36–76.

[11] C. Escauriaza, and F. Sotiropoulos, *Initial stages of erosion and bed form development in a turbulent flow around a cylindrical pier*, Journal of Geophysical Research: Earth Surface (2003–2012) 116 (2011).

[12] O. Link, C. González, M. Maldonado, and C. Escauriaza, *Coherent structure dynamics and sediment particle motion around a cylindrical pier in developing scour holes*, Acta Geophysica 60 (2012), pp. 1689–1719.

[13] Y.J. Chou, and O.B. Fringer, *A model for the simulation of coupled flow-bed form evolution in turbulent flows*, Journal of Geophysical Research: Oceans (1978–2012) 115 (2010).

[14] X. Yu, T.J. Hsu, and S. Balachandar, *A spectral-like turbulence-resolving scheme for fine sediment transport in the bottom boundary layer*, Computers & Geosciences 61 (2013), pp. 11–22.

[15] A. Khosronejad, and F. Sotiropoulos, *Numerical simulation of sand waves in a turbulent open channel flow*, Journal of Fluid Mechanics 753 (2014), pp. 150–216.

[16] P. Orlandi, *Vortex dipole rebound from a wall*, Physics of Fluids A: Fluid Dynamics (1989-1993) 2 (1990), pp. 1429–1436.

[17] T. Doligalski, C. Smith, and J. Walker, *Vortex interactions with walls*, Annual Review of Fluid Mechanics 26 (1994), pp. 573–616.

[18] O. Sano, T. Furuya, and B. Ito, *Collision of a vortex ring on granular layer*, in *IUTAM Symposium 150 Years of Vortex Dynamics (October 2008)*, 2008.

[19] R. Munro, N. Bethke, and S. Dalziel, *Sediment resuspension and erosion by vortex rings*, Physics of Fluids 21 (2009).

[20] N. Masuda, J. Yoshida, B. Ito, T. Furuya, and O. Sano, *Collision of a vortex ring on granular material. Part I. Interaction of the vortex ring with the granular layer*, Fluid Dynamics Research 44 (2012).

[21] J. Yoshida, N. Masuda, B. Ito, T. Furuya, and O. Sano, *Collision of a vortex ring on granular material. Part II. Erosion of the granular layer*, Fluid Dynamics Research 44 (2012).

[22] O. Desjardins, G. Blanquart, G. Balarac, and H. Pitsch, *High order conservative finite difference scheme for variable density low Mach number turbulent flows*, Journal of Computational Physics 227 (2008), pp. 7125–7159.

[23] P.A. Cundall, and O.D. Strack, *A discrete numerical model for granular assemblies*, Geotechnique 29 (1979), pp. 47–65.

[24] H. Zhu, Z. Zhou, R. Yang, and A. Yu, *Discrete particle simulation of particulate systems: theoretical developments*, Chemical Engineering Science 62 (2007), pp. 3378–3396.

[25] H. Zhu, Z. Zhou, R. Yang, and A. Yu, *Discrete particle simulation of particulate systems: A review of major applications and findings*, Chemical Engineering Science 63 (2008), pp. 5728–5770.

[26] J. Capecelatro, and O. Desjardins, *An Euler–Lagrange strategy for simulating particle-laden flows*, Journal of Computational Physics 238 (2013), pp. 1–31.

[27] J. Capecelatro, and O. Desjardins, *Eulerian–Lagrangian modeling of turbulent liquid–solid slurries in horizontal pipes*, International Journal of Multiphase Flow 55 (2013), pp. 64–79.

[28] J. Capecelatro, O. Desjardins, and R.O. Fox, *Numerical study of collisional particle dynamics in cluster-induced turbulence*, Journal of Fluid Mechanics 747 (2014), p. R2.

[29] P. Pepiot, and O. Desjardins, *Numerical analysis of the dynamics of two-and three-dimensional fluidized bed reactors using an Euler–Lagrange approach*, Powder Technology 220 (2012), pp. 104–121.

[30] N. Deen, M. Van Sint Annaland, M. Van der Hoef, and J. Kuipers, *Review of discrete particle modeling of fluidized beds*, Chemical Engineering Science 62 (2007), pp. 28–44.

[31] P. Zamankhan, *Analysis of submarine pipeline scour using large-eddy simulation of dense particle-liquid flows*, Journal of Offshore Mechanics and Arctic Engineering 131 (2009).

[32] O. Desjardins, G. Blanquart, G. Balarac, and H. Pitsch, *High order conservative finite difference scheme for variable density low Mach number turbulent flows*, Journal of Computational Physics 227 (2008), pp. 7125–7159.

[33] A.G. Kravchenko, H. Choi, and P. Moin, *On the relation of near-wall streamwise vortices to wall skin friction in turbulent boundary layers*, Physics of fluids. A, Fluid dynamics 5 (1993), pp. 3307–3309.

[34] R. Verzicco, and P. Orlandi, *A finite-difference scheme for three-dimensional incompressible flows in cylindrical coordinates*, Journal of Computational Physics 123 (1996), pp. 402–414.

[35] J. Lim, H. Choi, and J. Kim, *Control of streamwise vortices with uniform magnetic fluxes*, Physics of Fluids 10 (1998), pp. 1997–2005.

[36] W. Kramer, H. Clercx, and G. van Heijst, *Vorticity dynamics of a dipole colliding with a no-slip wall*, Physics of Fluids 19 (2007), p. 126603.